Title:

Structures of Langya virus fusion protein ectodomain in pre and post fusion conformation

Authors:

Aaron J. May[1,2], Karunakar Reddy Pothula[1], Katarzyna Janowska[1], Priyamvada Acharya[1,2,3]

Affiliations:

[1] Duke Human Vaccine Institute, Durham NC 27710, USA
[2] Duke University, Department of Biochemistry, Durham NC 27710, USA
[3] Duke University, Department of Surgery, Durham NC 27710, USA

[*]Correspondence: aaron.may@duke.edu (A.J.M), priyamvada.acharya@duke.edu (P.A.)

Abstract:

Langya virus (LayV) is a paramyxovirus in the *Henipavirus* genus, closely related to the deadly Nipah and Hendra viruses, that was identified in August 2022 through disease surveillance following animal exposure in eastern China. Paramyxoviruses present two glycoproteins on their surface, known as attachment and fusion proteins, that mediate entry into cells and constitute the primary antigenic targets for immune response. Here, we determine cryo-EM structures of the uncleaved LayV fusion protein (F) ectodomain in pre- and post-fusion conformations. The LayV-F protein exhibits pre- and post-fusion architectures that, despite being highly conserved across paramyxoviruses, show differences in their surface properties, in particular at the apex of the prefusion trimer, that may contribute to antigenic variability. While dramatic conformational changes were visualized between the pre- and post-fusion forms of the LayV-F protein, several domains remained invariant, held together by highly conserved disulfides. The LayV-F fusion peptide is buried within a highly conserved, hydrophobic, interprotomer pocket in the pre-fusion state and is notably less flexible than the rest of the protein, highlighting its "spring-loaded" state and suggesting that the mechanism of pre-to-post transition must involve perturbations to the pocket and release of the fusion peptide. Together, these results offer a structural basis for how the Langya virus fusion protein compares to its Henipavirus relatives and propose a mechanism for the initial step of pre- to post-fusion conversion that may apply more broadly to paramyxoviruses.

Importance:

The *Henipavirus* genus is quickly expanding into new animal hosts and geographic locations. This study compares the structure and antigenicity of the Langya virus fusion protein to other henipaviruses, which has important vaccine or therapeutic development implications. Furthermore, the study proposes a new mechanism to explain the early steps of the fusion initiation process that can be more broadly applied to the *Paramyxoviridae* family.

List of figures

Figure 1: Structure of LayV-F in pre- and post-fusion conformation.
Cryo-EM maps of the pre- and post-fusion conformations of LayV-F along with the fitted models with a sequence key.

Figure 2: Role of conserved cysteines during conformational conversion.
Demonstration of the role of conserved cysteines in each domain in pre- to post-fusion conformational changes.

Figure 3: Fusion peptide burial and conservation.
Exploration of motion in the pre-F structure through B-factor and DDM analysis with focus on the features and sequence conservation of the fusion peptide pocket.

Figure 4: Structure and antigenicity comparison of *Henipavirus* fusion proteins.
Comparison of LayV-F structure, surface residue types, and glycosylation pattern to previously determined NiV-F and HeV-F structures, with focus on important antigenic sites.

Figure 5: Fusion triggering hypothesis for paramyxoviruses.
Proposed mechanism of *Henipavirus* fusion triggering based on new data and previous knowledge.

Supplemental Figure 1: Sequence Alignment of *Paramyxoviridae* Fusion Proteins.
Color-coded sequence alignment of select *Paramyxoviridae* Fusion proteins compared to the LayV-F protein.

Supplemental Figure 2: Purification and Antibody Binding of *Henipavirus* Proteins.
Purification and quality control results for several *Henipavirus* fusion protein constructs with BLI binding data of anti-NiV antibodies against these constructs.

Supplemental Figure 3: Cryo-EM processing of LayV-F structures.
Cryo-EM processing of LayV-F in pre- and post-fusion conformation, showing representative micrographs, 2D classes, intermediate 3D refinements, and workflow.

Supplemental Figure 4: Fusion Peptide comparison.
Comparison of fusion peptide positions across several notable virus species.

Supplemental Figure 5: Fusion Peptide Pocket
Enlarged view of a panel from figure 3 depicting the fusion peptide burial pocket.

Figure Legends:

Figure 1: Structures of LayV-F in pre- and post-fusion conformation:

A-B. Cryo-EM reconstructions of LayV-F in **A.** pre- and **B.** post-fusion conformation, colored by protomer. Map regions colored in different shades of blue (pre-fusion) and yellow (post-fusion) for each protomer. Representative reference-free 2D classes used for the reconstruction are displayed above each map. **C-D.** Cartoon representation of atomic models of LayV-F in **C.** pre-fusion and **D.** post-fusion conformation that were built into the maps shown in **A-B**. In each, one protomer is colored by domain, based on the color scheme in panel **E**, and the other two protomers colored gray. **E.** Sequence domain key for LayV-F. SS: Secretion signal, cleaved prior to purification. DI, DII, DIII: Domains I, II, and III. FP: Fusion Peptide. HRA, HRB: Heptad repeats A and B. Foldon: Trimerization domain. TS: Twin-Strep tag, used for purification with modified streptavidin resin.

Figure 2: Role of conserved cysteines during conformational conversion.

A. Zoomed-in view of the DIII domain, including the fusion peptide (orange) and HRA (yellow), shown for the (left) pre- and (right) post-fusion structures. Color scheme continued from Figure 1E. The cleavage site at R104 is identified, as well as the disulfide bond formed by C66 and C187 (yellow sticks). This disulfide bond is a hinge point around which the HRA straightens into the central coiled-coil in the post-fusion F structure. **B-C.** Superimposition of pre- and post-fusion conformation domains DI (**B**) and DII (**C**). Color scheme continued from figure 1E, with the post-fusion conformation colored in a lighter shade. Disulfide bonds are shown as yellow sticks and labelled. For DII, the movement of the HRB linker region is indicated by an arrow. **D.** Sequence alignment of paramyxovirus fusion proteins in the regions surrounding conserved cysteines, with cysteine residue number and domain labelled. Viruses colored blue are from the *Henipavirus* genus and colored tan for other paramyxoviruses. Residues are colored by type, per MView standard (1). Blue: Alcohol, Green: Hydrophobic, Dark Blue: Negative charge, Red: Positive charge, Purple: Polar, Yellow: Cysteine.

Figure 3: Fusion peptide burial and conservation.

A. Structure of the pre-fusion LayV-F protein shown in cartoon representation and colored by B-factors. **B.** Difference Distance Matrix plot comparing relative residue positions between pre-fusion and post-fusion conformation. Sequence key from figure 1E included along each axis. Gray areas in the bottom right half of the plot are the result of sequences not present in the post-fusion model. **C.** Hydrophobic fusion peptide pocket in pre-fusion state, with fusion peptide depicted as orange cartoon, and surface electrostatics view of the pocket. **D.** Side-chain stick view of the fusion peptide pocket, with hydrophobic residues involved shown with side chains as green sticks. An enlarged view of this panel with residues labeled is seen in supplemental figure S5. **E.** Cartoon representations of a single pre-fusion state protomer, colored by sequence conservation across *Henipavirus* fusion proteins. Color scale generated by ChimeraX default AL2CO entropy measure. **F.** Zoom in of the fusion peptide pocket, colored by sequence

conservation as in H. The fusion peptide pocket is among the most strongly conserved region of the protein.

Figure 4: Structure and antigenicity comparison of Henipavirus fusion proteins.

A. Superimposition of a single pre-fusion protomer of LayV-F (blue) NiV-F (cyan) and HeV-F (green), in cartoon representation. PDBs: LayV-F: 8FEJ, NiV-F: 5EVM, HeV-F: 5EJB (2, 3). **B.** Zoomed in view of a loop within the folded HRA, one of the few areas of significant structural difference between LayV-F and NiV/HeV-F. **C.** Binding site of known paramyxovirus F protein-neutralizing antibodies, labeled by the species targeted. NiV-F trimer from 12B2-bound structure shown as cartoon and antibody Fabs shown in surface view. Only one Fab per type shown, all expect PIA174 bind with 3:1 stoichiometry. PDBs: PIA174: 6MJZ, 12B2: 7KI4, mAb66: 6T3F, 1F5: 7KI6, 5B3: 6TYS (4-6). **D.** Surface view of LayV-F and NiV-F with glycosylation sites (residues meeting the N-X-S/T glycosylation sequence) colored teal. **E.** Surface representation of LayV-F colored by sequence conservation across *Henipavirus* fusion proteins. Color scale generated by ChimeraX default AL2CO entropy measure; magenta indicates high conservation and teal indicates high variability (7). **F.** Surface representation of paramyxovirus fusion proteins, showing only main chain atoms, colored by residue type and shown from top-down view. Tan: hydrophobic, Pink: polar, Red: negative, Blue: positive, teal: Potential glycosylation. PIV5 PBD: 4GIP (8).

Figure 5: Fusion triggering hypothesis for paramyxoviruses.

A. Existing model of *Henipavirus* (HNV) fusion protein triggering based on Liu *et al.* (2013) (9). HNV-G, brown, shown in a two-receptor binding domain down “closed” state, bound to HNV-F in pre-fusion conformation. Exposure to Ephrin B2/B3 receptor induces opening of HNV-G, triggering conversion of HNV-F from pre-fusion to the pre-hairpin state. The triggering interaction is labeled with a star. **B.** Hypothesized structural basis for the G-F interaction shown in **A**, wherein a two-step mechanism involving disruption of the fusion peptide burial pocket through action of the HNV-G stalk on DII frees the fusion peptide, allowing conformational conversion.

Supplemental Figure 1: Sequence Alignment of *Paramyxoviridae* Fusion Proteins.

Sequence alignment of select paramyxovirus fusion proteins with LayV-F used as the reference sequence. Cov: percent sequence coverage. Pid: percent sequence identity. Residues are colored by type, per MView standard (1). Blue: Alcohol, Green: Hydrophobic, Dark Blue: Negative charge, Red: Positive charge, Purple: Polar, Yellow: Cysteine. Consensus residue types assigned per MView standard. Alcohol: (o), Aliphatic: (l), Aromatic: (a), Charged: (c), Hydrophobic: (h), Negative: (-), Polar: (p), Positive: (+), Small: (s), Tiny: (u), Turnlike: (t).

Supplemental Figure 2: Purification and Antibody Binding of *Henipavirus* Proteins.

A. Size-exclusion chromatogram of *Henipavirus* fusion protein purification. LayV-F, blue, NiV-F WT, dashed red, pre-fusion stabilized NiVop08 (10), dashed green. The fractions identified as the ectodomain trimer at 180kDa are indicated with a vertical dashed line **B.** Differential scanning fluorimetry profiles of the products from A, LayV-F measured in triplicate. **C-E.** SDS-

PAGE of *Henipavirus* constructs from A. Molecular weight markers, MW, non-reducing conditions, NR, reducing conditions, R., **C.** LayV-F loaded at 1µg per lane. **D.** LayV-F loaded at 8µg per lane. **E.** NiVop08 loaded at 3µg per lane, with left two bands sampling the first peak at 440kDa and the second two bands sampling the trimer peak at 180kDa. **F.** BLI sensorgram of anti-NiV-F antibodies h5B3.1 and 12B2 binding to immobilized LayV-F or NiVop08 (6, 11).

Supplemental Figure 3: Cryo-EM processing of LayV-F structures.

Cryo-EM processing of pre- and post-fusion LayV-F structures. Steps performed using CryoSPARC (12, 13). CTF Estimation performed on micrographs followed by default blob picker algorithm and a trained AI-based algorithm (Topaz) for particle picking. Particles for the post-fusion state were obtained through the blob picker, while particles contributing to the pre-fusion state came from both sets. Heterogeneous refinement was used to classify and further sort particles. After non-uniform refinement, a local refinement was performed on the entire structure. The supplemental map of the post-fusion state prior to local refinement where the N65 glycan is detected has also been deposited.

Supplemental Figure 4: Fusion Peptide comparison.

A-E: Comparison of fusion peptide location in other viral fusion proteins. In the top portion of each panel, fusion proteins are shown in cartoon representation in gray, with the fusion peptide as orange spheres, and in the bottom portion, fusion peptides are shown as cartoon representation with side chains as sticks, orange, with the surface of the rest of the fusion protein colored based on protomer. The most proximal protomer to the highlighted fusion peptide is colored cyan, with the neighboring protomers colored green and tan. In cases where there are are multiple subunits in the fusion protein, the attachment subunit is colored a darker shade than the corresponding fusion subunit. **A.** HIV Envelope (Env) closed conformation, with (PDB: 4TVP) and without fusion peptide-targeting antibody VRC34.01 (PDB: 5I8H), shown in cartoon, red. **B**. HIV Env in open conformation (PDB: 5VN3). **C.** Influenza HA in closed conformation (PDB: 6HJN). **D.** SARS-CoV-2 Spike in pre-fusion, receptor-binding domain down conformation (PDB: 6XR8). **E.** Ebola GP in pre-fusion conformation (PDB: 3CSY). (14-19)

Supplemental Figure 5: Fusion Peptide Pocket

Enlarged view of figure 3D. Side-chain stick view of the fusion peptide pocket, with hydrophobic residues involved labelled and shown with side chains as green sticks.

Supplemental Note 1.

Comparison of the LayV-F fusion peptide (FP) arrangement to other viral fusion peptides highlights the unique nature of the paramyxovirus FP. Whereas a large portion of the LayV-F FP is buried within an interprotomer pocket, the HIV envelope protein (Env), the FP remains largely surface exposed in the closed conformation (Supplemental Figure 4A) (19). The most N-terminal residues of the HIV-1 FP are often unresolved in structures, further highlighting the flexibility of the FP in this Env conformation. During receptor-induced Env opening, the FP begins to be pulled into the core of the protein, and though not buried, it has a somewhat lesser degree of surface exposure (Supplemental Figure 4B) (18). In contrast, the Influenza Hemagglutinin protein (HA), in the pre-fusion state, maintains the N-terminal end of the FP in a hydrophobic cavity at the core of the protein (Supplemental Figure 4C) (16). While the Influenza HA FP is not mobile and flexible as with the HIV-1 FP in the closed state of Env, the Influenza HA FP arrangement does not constitute as true burial, as the FP is inserted into a recess in the structure but not occluded by other residues. The exact nature of the SARS-CoV-2 spike FP is uncertain, as several regions in S2 may play a role. Many structures have identified the stretch of residues directly following the S2' cleavage site as the fusion peptide. This region is not buried, and like the FP of HIV Env, is often poorly resolved in spike structures (Supplemental Figure 4D) (15). However, a recent study (20) indicates that it is residues 866-910 that insert into the host membrane. Close examination of the SARS-CoV-2 sequence reveals that the residues that in the middle of this FP region, which form an internal FP, much more closely matching the glycine and alanine-rich sequences of other known FPs than those directly following the S2' site. This FP arrangement has a much greater degree of similarity in pre-fusion arrangement to paramyxoviruses. The FP region is almost completely buried by the surrounding domain and has limited surface accessibility (Supplemental Figure 4D). While this FP burial is more comparable to paramyxoviruses, the usage of an internal FP loop draws a comparison to the Ebola glycoprotein (GP) FP, also an internal FP. This Ebola FP region is not buried in the GP structure, instead forming the exterior of the fusion subunit. Though it is an internal FP, as with SARS-CoV-2, the fusion loop is positioned between two beta strands rather than two alpha helices (Supplemental Figure 4E) (14).

Introduction

Langya virus (LayV) is a newly identified member of the *Henipavirus* genus, detected after surveillance of disease following animal exposure in eastern China (21). Over the course of several years, LayV infections were identified in 35 individuals, 26 of whom were infected solely with LayV. In these 26 individuals, common symptoms included fever, fatigue, cough, nausea, and headaches. The genome organization of LayV is identical to that of other henipaviruses, including the better known and highly virulent Nipah and Hendra viruses. Based on phylogenetic analysis, LayV is most closely related to Mojiang virus (MojV), which was discovered in rats in southern China (22), and Gamak (GAKV) and Daeryong (DARV) viruses, which were detected in shrews in the Republic of Korea (23).

The henipaviruses infect a range of animals with Nipah and Hendra viruses having their natural reservoir in fruit bats (24). However, several additional *Henipavirus* species have been discovered in recent years with differing animal reservoirs. A survey of both domestic and wild animals revealed a low level of seropositivity for LayV in goats and dogs (2% and 5% respectively) and the highest positivity rate (52.1%) in shrews (*Crocidura lasiura* specifically), indicating that shrews may be the natural reservoir for LayV. The *Henipavirus* genus is a member of the *Paramyxoviridae* family (25), which includes both extremely infectious human pathogens, such as measles and mumps, and extremely deadly pathogens, such as Nipah and Hendra. This diversity of infectivity and virulence, as well as diversity of animal reservoirs are risk factors that necessitate paramyxovirus research. Accordingly, Nipah and Hendra virus are listed as priority pathogens by the WHO (26).

Henipaviruses present two surface glycoproteins known as the attachment and fusion proteins. These proteins work together to mediate viral entry into host cells and in Nipah virus both have been shown to be required for viral entry (27). As these are the sole virus surface-expressed proteins, they are also the primary targets of neutralizing antibodies against henipaviruses. The *Henipavirus* attachment protein has receptor-binding capability and, in Nipah and Hendra viruses, binds to Ephrin B2 and B3, which is found mostly in the brain and in endothelial cells in the heart and lungs (28, 29). The *Henipavirus* fusion (F) protein is a class-I fusion protein that has a metastable pre-fusion conformation which is displayed on virion

surfaces prior to receptor engagement and a post-fusion conformation that is adopted after virus-cell fusion (30, 31). Proteolytic cleavage splits F into two subunits, F_1 and F_2, still connected by disulfide linkages (30, 32), freeing a series of hydrophobic residues known as the fusion peptide to be inserted into the host cell membrane during this conformational conversion. This process anchors the virus to the host cell and allows the formation of a six-helix bundle in the F protein to bring the viral and host membranes together, facilitating fusion. Although it has many mechanistic features in common with other class-I fusion proteins, the F protein in paramyxoviruses does not appear to have any primary receptor-binding functionality. This role is fulfilled by a separate attachment glycoprotein, which is believed to undergo conformational changes during receptor binding which pass a triggering signal to F (33, 34). The structural basis for this process is poorly understood.

Here, we determine cryo-EM structures of the LayV fusion protein (LayV-F) in pre- and post-fusion conformations, both at 4.64Å resolution. The LayV-F ectodomain sequence as reported by Zhang *et al*. (2022) was used (21), replacing the transmembrane and cytoplasmic domains with purification tags and a trimerization domain. No prefusion stabilizing mutations were made, nor was the fusion protein cleaved or otherwise knowingly induced to convert to the post-fusion state. We compare it to other known *Henipavirus* fusion protein structures and elucidate the structural basis for pre- to post-fusion conversion in both LayV and more broadly for *Henipavirus* fusion proteins. Our study demonstrates that the highly conserved paramyxovirus fusion protein architecture is utilized by LayV-F, identifies a region of variability among *Henipavirus* fusion proteins in an important antigenic site, and provides evidence for a mechanism to describe how *Henipavirus* fusion proteins are triggered to undergo conformational changes during the fusion process.

Results

Purification and Structural Determination of LayV-F

We purified the LayV-F ectodomain based on protocols previously developed for NiV-F, by expressing in 293F cells and purifying via StrepTactin (IBA lifesciences) affinity chromatography followed by size exclusion chromatography. Like the NiV-F protein, the LayV F ectodomain elutes with a distinct peak at ~180 kDa. Higher molecular weight species, broader than the main peak, were also observed at ~400 kDa and above (Supplemental Figure 2A). These could be the result of low-affinity interactions between individual trimers. SDS-PAGE analysis of these high molecular weight species in both NiV-F and LayV-F purifications has consistently produced identical bands corresponding to the ~180 kDa species, consistent with the uncleaved F protein (Supplemental Figure 2E). Higher order multimers of Henipavirus F proteins with rings described as "hexamers of trimers" have been previously reported (2). While larger molecular weight species were detected during purification of LayV-F (Supplemental Figure 2A), they comprised a far lower proportion of total protein as compared to purifications of wild-type NiV-F and a prefusion-stabilized NiV-F mutant, NiVop08 (Supplemental Figure 2A) (10). The yield of LayV-F at ~1.2mg/L was considerably higher than that of wild-type NiV-F at ~250µg/L. The NiVop08 yield was vastly higher than the unstabilized NiV-F construct at ~3mg/L, consistent with the general trend of prefusion-stabilized fusion protein constructs expressing more efficiently than their wild-type counterparts (35-38). Differential scanning fluorimetry (DSF) suggested reduced stability of LayV-F compared to NiV-F (Supplemental Figure 2B). The LayV-F DSF profile closely resembles that of wild-type NiV-F, but is left-shifted, indicating that the temperature-induced conformational changes or unfolding events are occurring at a lower temperature for LayV-F.

We determined the structure of the LayV-F ectodomain trimer using cryo-EM. Reference-free 2D classes revealed both pre- and post-fusion conformations of LayV-F in the cryo-EM dataset (Figure 1A-B). After several rounds of classification and sorting we obtained 4.64 Å reconstructions (calculated within cryoSparc according to the FSC 0.143 gold-standard criterion) of the pre-fusion and post-fusion forms of the LayV F protein from approximately 200,000 and 80,000 particles, respectively. Assessment of the three-dimensional FSC (3DFSC) plot for these maps indicated resolutions of 5.42 Å and 5.25 Å for the pre- and post-fusion conformations,

respectively (39). The structures determined revealed pre- and post-fusion architectures that were similar to those determined for other paramyxoviruses (2-4, 8, 40, 41). The pre-fusion LayV F structure has a compact "clove-like" shape with a large internal cavity and spans ~110 Å from the bottom of the stalk to the top of the apex. In comparison, the post-fusion structure is elongated, spanning ~160 Å, with regions that formed the pre-fusion apex straightening into a central coiled-coil, ending with the trademark six-helix bundle of the post-fusion conformation.

The LayV F ectodomain includes a fusion peptide (FP) and two heptad repeat sequences that both contribute to three domains, previously described by Yin *et al*. for the parainfluenzavirus 5 (PIV5) F protein (Figure 1C-E) (41). Domain I (DI) is comprised of the most N-terminal residues after cleavage of the signal peptide, 22-45, and residues 278-369. Its central β-sheet connects Domain II (DII) to the apical Domain III (DIII). DII, from residues 370-446, makes significant contact with the cleavage site and fusion peptide of the neighboring protomer before leading to heptad repeat B (HRB), located at the most C-terminal end of the ectodomain. DIII, from residues 46-277, contains the cleavage site, fusion peptide, and heptad repeat A (HRA) (Figure 1C-E). Residues 93-140 from DIII and 441-450 from DII, which become linker regions leading to the repositioned heptad repeats now forming the six-helix bundle, are not resolved in the post-fusion structure (Figure 1E).

<u>Pre- to post-fusion Conversion Mechanism of LayV-F</u>

Though the *Henipavirus* genus was established with the discovery of Hendra virus in 1994 (24, 42), the number of members of the genus has dramatically expanded in recent years with the discovery not only of Langya virus, but also Gamak and Daeryong virus, both identified in 2021 (23). Within the past three years, Henipaviruses have been identified in an expanded range of animal hosts and geographic locations. No longer contained to southeast Asia and Australia, new species have been discovered in Africa and South America, specifically Angavokely virus and Peixe-Boi virus, respectively (43, 44). Although there is very high structural similarity for fusion proteins across not only the *Henipavirus* genus, but within the larger *Paramyxoviridae* family, there tends to be low sequence identity between species, with LayV-F having ~40% sequence identity with NiV-F, and ~30% or less identity to other non-*Henipavirus* paramyxoviruses (Supplemental Figure 1). However, with more *Henipavirus* members identified, some conserved

sequence features have become more evident. These include 10 highly conserved cysteines present in the ectodomain of paramyxovirus F proteins (Figure 2). Identifying the locations of these cysteines in the pre- and post-fusion LayV-F structures reveals their critical role in maintaining domain fold integrity during the dramatic conformational changes that occur during fusion.

Despite the drastically different shapes of the pre- and post-fusion conformations of LayV-F resulting in a 51.6 Å Cα RMSD, superimposition of the DI and DII domains demonstrates that these domains remain largely invariant through the pre- to post-fusion transition of the F protein (Figures 2A-C). Both DI and DII domains have two internal pairs of disulfide bonds that help maintain the rigidity of these domains (Figure 2B-D). DI shows a pre- to post-fusion Cα RMSD of 2.16 Å, while DII undergoes more total movement, resulting in pre- to post-fusion Cα RMSD of 16.5 Å with the linker region from S423 to I446 that leads to HRB extending away from the domain as HRB moves to its post-fusion location (Figure 2C). Excluding these residues from the RMSD calculations, DII shifts only 2.3 Å. The difference in conformation of DIII from pre- to post-fusion is more dramatic. Based on sequence alignment, the F_1-F_2 cleavage site for LayV-F is expected to be immediately after the highly conserved residue R104 (Supplemental Figure 1), however cleavage did not occur in this construct (Supplemental Figure 2C-D). The largest positional shifts during the pre- to post-fusion transition occurred in the fusion peptide and HRA, which extend and continue the along the path of the apical helix, now forming the central coiled-coil (Figure 1A). These movements occur around a hinge point in DIII where the apical helix is connected to the rest of DIII by a disulfide bond, again demonstrating the role of the conserved cysteines in providing an anchor for large conformational changes in the F protein (Figure 2A).

Fusion triggering Mechanism of *Henipavirus* Fusion proteins

Insertion of the hydrophobic fusion peptide (FP) into the host membrane is an essential step that leads to the fusion of the virus and host cell membranes. In the pre-fusion LayV-F, a substantial portion of the FP is buried within a pocket formed between two LayV-F protomers, requiring the FP to be released from this pocket during the pre-to-post fusion conformational transition (Figure 3). Hydrophobic residues lining the interprotomer pocket into which the FP is buried in the pre-fusion LayV-F include L51, L89, M92, L93, V96, V216, and I262 from DIII,

A108, M110, G112, A114, L115, and G116 from the N-terminal end of the FP upstream of the helical segment from the same protomer, and residues from the adjacent protomer include M292 from DI and P369, F371, A372, L373, G376, V378, I420, L421, and I422 from DII (Figure 3D, Supplemental figure 5).

Consistent with the close packing of the FP within an interprotomer pocket in the pre-fusion F conformation, the modeled coordinates exhibit the lowest B-factors at the FP, while HRB, its DII linker, and surrounding DI region have the highest B-factors in the structure (Figure 3A). The HRA, HRB and FP undergo dramatic shifts in their positions during pre- to post-fusion conformational change of the LayV-F protein (Figure 3B). Although the FP is not resolved in the post-fusion state, based on its location it is expected to show a position shift similar to that of HRA. The burial of the pre-fusion FP and its interactions with the residues lining the interprotomer pocket suggest that the purpose of this pocket is to hold the FP in place to prevent premature conversion to the post-fusion form and therefore is the source of metastability of the pre-fusion LayV F structure. Consistent with a key role in pre-to post-fusion conformational dynamics, the FP and the surrounding pocket are among the most conserved regions in *Henipavirus* fusion proteins (Figure 3E-F). Release of the FP from this pocket is a requirement for the conformation transition of the F protein from the pre-fusion to post-fusion conformation and disruption of this pocket may be the mechanism by which the FP is released to undergo these changes.

Structural Conservation and Antigenic Diversity of *Henipavirus* Fusion proteins

Despite low overall sequence conservation, the structural similarity of paramyxovirus fusion proteins is striking. Structures have previously been determined for the F proteins of two *Henipaviruses* in the pre-fusion state, NiV-F and HeV-F (2, 3). Despite having only 38% sequence identity with these viruses, a superimposition of LayV-F with these structures reveals a conserved architecture (Figure 4A), with Cα RMSDs of 2.64 Å and 3.00 Å for LayV-F to NiV-F and HeV-F, respectively, with NiV-F and HeV-F differing between each other by 0.94 Å. One of the few areas between these species where there is a notable shift is in HRA. In the pre-fusion conformation, the central helix in HRA is broken by a short, two-strand beta sheet with a loop that extends to the exterior of the protein. As compared to the homologous HRA loop in

NiV/HeV-F, in LayV-F there is a shift of ~9 Å in the direction of the fusion peptide (Figure 4B). It is unclear if this shift results in any mechanistic effect on the HRA region, although the loop resides within a site targeted by antibodies and shift in its position may alter antigenicity of the F protein. (Figure 4C).

An overlay of all experimentally determined structures of paramyxovirus-targeted antibodies highlights the antigenicity of the HRA loop site and its adjacent regions (Figure 4C). Several antibodies target DIII in the pre-fusion F near the HRA region and likely interfere with pre- to post-fusion conversion. In addition to the HRA loop shift described above, LayV-F and other paramyxovirus species show differences in their surface-exposed residues in these regions that could define the unique antigenic properties of the different F proteins. These include a glycosylation site in LayV-F at N279 (Figure 4D), which is positioned between DI and DIII near several of the previously identified epitopes, specifically 15F, an HeV-neutralizing antibody and 5B3, a cross-reactive NiV/HeV-neutralizing antibody (6).

The sequences of both NiV-F and HeV-F have two plausible glycosylation sites at N64 and N67, both at the apex, though previous studies have established that only N67 is glycosylated (45, 46). The N65 glycosylation position in LayV-F is shifted by 8.2 Å away from the apex residues of HRA. This glycan was particularly visible in the cryo-EM reconstructions of the post-fusion conformation before local refinement, where the density at roughly the half-height point of the map corresponds to N65 (Supplemental Figure 3). Interestingly, sequence alignment reveals that the LayV-F N65 glycosylation site is not homologous to either N64 or N67 of NiV/HeV, but rather is equivalent to residue 70 (Supplemental Figure 1). Viewing the fusion protein colored by sequence conservation further highlights the variability of this region (Figure 4E). While there are highly conserved residues at discrete points of the surface, namely the highly conserved disulfide bond near the apex, the surrounding region ranges from moderately conserved to highly variable, especially in surface-accessible regions of DIII and the HRA loop. This variability includes differing residue types between LayV and other henipaviruses, particularly at the apex site. The differences in the pre-fusion F protein trimer apex are highlighted by a negatively charged residue, D188, in both NiV and HeV, while the LayV-F protein instead has polar residues (N183, Q184) and an overall greater hydrophobic character.

This residue arrangement in the pre-fusion LayV-F trimer apex is more similar to that of the PIV5 pre-fusion F protein (Figure 4F). This change in residue type is likely a source of antigenic variability between paramyxovirus F proteins. Consistent with this variability, antibody 12B2, that binds an epitope in pre-fusion NiV-F that includes the trimer apex (6, 11), did not show binding to LayV-F (supplemental Figure 2F). Therefore, despite similar F protein architecture, antigenic variability within paramyxoviruses is driven by variability of surface residues.

Discussion

The continuing emergence of new paramyxovirus species necessitates heightened focus on a family that includes both some of the world's deadliest pathogens in Nipah virus, and most infectious in measles and mumps. Members specifically of the *Henipavirus* genus have spread to humans through zoonotic transfer. While Nipah and Hendra viruses are spread to humans through bats, new henipaviruses have been detected in a range of species, such as shrews and rats. The role of animal reservoirs in the SARS-CoV-2 pandemic highlights the risk factor that a diverse range of animal hosts can be, further necessitating efforts to develop treatments or vaccines against henipaviruses. Structural determinations of *Henipavirus* glycoproteins serve as a foundation for future immunogen or therapeutic design.

Though the structure of LayV-F is strikingly similar to other known *Henipavirus* F structures, key differences in surface characteristics at the apex have implications for pan-*Henipavirus* or pan-paramyxovirus vaccine development. When developing vaccinations for a virus that is quickly mutating, or with many distinct strains, as observed with henipaviruses, it is advisable to target relatively invariable sites for immunogen design. Our pre-fusion LayV-F protein structure helps to demonstrate the particularly variable nature of the apex and DIII in *Henipavirus* F proteins, a trait to be considered when selecting antigenic sites to target for a broad immunogenic response.

In contrast to existing structures of paramyxovirus fusion proteins that were determined in either pre- or post-fusion conformation, our study resolves the LayV-F pre- and post-fusion structures within the same cryo-EM dataset, suggesting that for LayV-F, being in solution at ambient temperatures may allow the proteins to sample enough conformational states such that some will lead to conversion. Though paramyxovirus fusion proteins must be cleaved to enable fusion peptide insertion, prior studies have observed uncleaved fusion proteins assuming a post-fusion conformation (47). Our structures reveal a highly stable configuration of the fusion peptide (FP) in the pre-fusion F conformation, buried within an interprotomer pocket, which must be disrupted to transition to the post-fusion conformation. These observations suggest that FP configuration is a source of metastability in the pre-fusion LayV-F protein, where a shift in the position of the FP or the residues surrounding it in the interprotomer pocket too far from its

pre-fusion configuration may lead to irreversible conversion to the post-fusion form. This, together with the biochemical properties of the FP burial pocket, suggests tight control of FP positioning is an important part of pre-fusion metastability.

An elusive question regarding paramyxovirus fusion is how the fusion process is first initiated. For the many virus families that utilize a fusion protein, the metastable pre-fusion state is maintained prior to a triggering event that initiates conformational changes. In many cases, this process involves cleavage and removal of entire domains of the fusion protein, such as with the removal of the S1 subunit from the SARS-CoV-2 spike protein prior to fusion. The paramyxovirus fusion proteins, however, have no such attachment subunit to remove. Instead, paramyxoviruses utilize a separate attachment protein, which is thought to pass on a triggering signal to the fusion protein after receptor binding (33, 34) (Figure 5A). Within the *Henipavirus* and *Morbilivirus* genera, the attachment and fusion proteins are believed to form complexes prior to receptor engagement (33) (Figure 5A). While this might suggest a mechanism where the attachment protein functions as a clamp on the fusion protein, maintaining the pre-fusion state before receptor binding, studies assaying fusion competency have demonstrated that the fusion protein alone is not sufficient for virus and host cell fusion, indicating that fusion triggering involves a more complex mechanism of interaction between the two proteins (9, 48).

The fusion peptide in the pre-fusion LayV-F protein is in a configuration that is conserved among paramyxoviruses and distinct from other class-I fusion proteins (Supplemental Figure 5, Supplemental Note 1). It is not yet known which residues are involved in the interaction between the attachment and fusion proteins, but the critical role of the FP pocket created at the DII-DIII interface suggests that DII could be the site of the interaction. The triggering signal may be transferred by way of the attachment protein repositioning DII such that the fusion peptide is released from the pocket, irreversibly extending towards the apex (Figure 5B). This mechanism would be consistent with previous paramyxovirus studies that suggested an attachment protein-binding role for DII (49, 50). Further supporting this hypothesis is the likelihood that the FP in the pre-fusion conformation is in a high-energy state due to the kink in the helix comprised of the FP from T119 through HRA up to N148. Such a helix shape is often brought about by the presence of a proline at the kink, introducing bond-angle limitations that force this shape into the

helix (51). However, in the helix containing the FP, no proline is present. The bent shape could be induced by the FP being buried within and locked into the hydrophobic FP pocket. When disrupted, the position of the FP would therefore move rapidly as the tension in the helix is resolved. Though it could be hypothesized that cleavage of the FP is the trigger that allows for rearrangement, our study, in line with others, has established that cleavage is not required for conformational conversion in paramyxovirus fusion proteins. The existence of a high-energy state FP helix, held in place by an interprotomer DII, which is then disrupted by the action of an attachment protein offers a logical explanation for how *Henipavirus* attachment proteins activate their conjugate fusion proteins, and establishes the basis for how paramyxovirus fusion proteins maintain their metastability in the pre-fusion state.

Materials and Methods

Data Availability. Cryo-EM reconstructions and atomic models generated during this study are available at wwPDB and EMBD (https://www.rcsb.org; http://emsearch.rutgers.edu) under the accession codes PDB IDs 8FEJ and 8FEL and EMDB IDs EMD-29029 and EMD-29032.

Plasmids. Gene synthesis for all plasmids generated by this study were performed and the sequence confirmed by GeneImmune Biotechnology (Rockville, MD). The fusion protein ectodomain constructs included F protein residues 1 to 438 (GenBank: UUV47205.1), a C-terminal T4 fibritin trimerization motif (FOLDON), a C-terminal HRV3C protease cleavage site, a TwinStrepTag and an 8XHisTag. The ectodomain was cloned into the mammalian expression vector pαH. Synthetic heavy and light chain variable domain genes for Fabs were cloned into a modified pVRC8400 expression vector, as previously described (5, 24, 25). Antibody variable regions for both heavy and light chain replaced the variable regions from the VRC01 antibody plasmid (52), with the IL-2 secretion signal and human kappa constant domain being used for light chain plasmids. All plasmids have been deposited to Addgene (https://www.addgene.org) under the codes XXX.

Cell culture and protein expression. For F ectodomains, GIBCO FreeStyle 293-F cells (embryonal, human kidney) were maintained at 37°C and 9% CO_2 in a 75% humidified atmosphere in FreeStyle 293 Expression Medium (GIBCO). The Plasmid was transiently transfected using Turbo293 (SpeedBiosystems) and incubated at 37°C, 9% CO2, 75% humidity with agitation at 120 rpm for 6 days. On the day following transfection, HyClone CDM4HEK293 media (Cytiva, MA) was added to the cells. For antibodies, GIBCO Expi293F cells (embryonal, human kidney) were maintained at 37°C and 9% CO_2 in a 75% humidified atmosphere in Expi293 Expression Medium (GIBCO). The Plasmid was transiently transfected using Expifectamine 293 (GIBCO) and incubated at 37°C, 9% CO2, 75% humidity with agitation at 120 rpm for 6 days. On the day following transfection, Expifectamine 293 Enhancers (GIBCO) were added to the cells.

Protein purification. On the 6th day post transfection, the fusion protein ectodomains were harvested from the concentrated supernatant, purified using StrepTactin resin (IBA LifeSciences) and size exclusion chromatography (SEC) using a Superose 6 10/300 GL Increase column (Cytiva, MA) equilibrated in PBS buffer (Thermo Scientific 137mM NaCl, 2.7mM KCl, pH 7.4, 10 mM Phosphate Buffer, 1.8mM Potassium Phosphate Monobasic). Antibodies were purified using Protein A affinity (Thermo Scientific) and SEC using a Superose 6 10/300 GL Increase column (Cytiva, MA) equilibrated in PBS buffer (Thermo Scientific 137mM NaCl, 2.7mM KCl, pH 7.4, 10 mM Phosphate Buffer, 1.8mM Potassium Phosphate Monobasic). All steps of the purification were performed at room temperature and in a single day. Protein quality was assessed by SDS-Page using NuPage 4-12% (Invitrogen, CA). The purified proteins were flash frozen and stored at -80 °C in single-use aliquots. Each aliquot was thawed by a 5-minute incubation at 37 °C before use.

Cryo-EM. Purified ectodomain was diluted to a concentration of 1.5 mg/mL in PBS (described above) with 0.0005% DDS and 0.38% glycerol added. A 2.2µL drop of protein was deposited on a Quantifoil R1.2/1.3 grid (Electron Microscopy Sciences, PA) that had been glow discharged for 10 seconds using a PELCO easiGlow™ Glow Discharge Cleaning System. After a 30-second incubation in >95% humidity, excess protein was blotted away for 2.5 seconds before being

plunge frozen into liquid ethane using a Leica EM GP2 plunge freezer (Leica Microsystems). Frozen grids were imaged using a Titan Krios (Thermo Fisher) equipped with a K3 detector (Gatan). Movie frame alignment was carried out using UNBLUR (53).The cryoSPARC (12) software was used for data processing. Phenix (54), PyMOL(55), ChimeraX (56) and Isolde (57) were used for model building and refinement. Phenix was first used to fit the initial models into maps. ISOLDE was used to manually adjust residues to address rotamer and Ramachandran outliers. Phenix was again used to perform real-space refinement, energy-minimization of side-chain positions, and to set B-factors during an ADP-only real-space refinement.

SDS-PAGE. Prepared 1, 3, or 8µg of sample with Laemmli sample buffer (BioRad), PBS buffer, and with or without 300mM DTT (Reduced/Non-Reduced). Loaded to NuPAGE 4-12% Bis-Tris gel (Invitrogen) and ran at 175V with MES-SDS running buffer until complete. Stained with Coomassie blue (Novex) for 30 minutes before water destain and imaging.

Differential scanning fluorimetry. DSF assay was performed using Tycho NT. 6 (NanoTemper Technologies). Spike ectodomains were diluted to approximately 0.15 mg/mL. Intrinsic fluorescence was measured at 330 nm and 350 nm while the sample was heated from 35 to 95 °C at a rate of 30°C/min. The ratio of fluorescence (350/330 nm) and inflection temperatures (Ti) were calculated by the Tycho NT. 6 apparatus.

Difference distance matrices (DDM). DDM plots were generated using the Bio3D package (Grant *et al*., 2021) implemented in R (R Core Team, 2018. R: A language and environment for statistical computing. R Foundation for Statistical Computing, Vienna, Austria. http://www.R-project.org/).

Bio-layer Interferometry (BLI). Antibody binding to *Henipavirus* F proteins was assessed using BLI on an Octet RED 384 (Sartorius, formerly ForteBio) with Forte Bio Kinetics Buffer. All binding assays were performed at 30°C. Antibodies were immobilized on Anti-Human Fc Capture tips (ForteBio), loaded at 20µg/mL for 300s. F proteins were used as analytes at 100nM, with an association time of 480s and dissociation time of 600s. Sensorgram data were reference-subtracted and analyzed using the Octet Analysis Studio software (Sartorius), with a reference tip for each immobilized antibody and reference sample for each analyte.

Sequence Alignment. Paramyxovirus F sequences aligned with Clustal Omega tool (58). Output alignment was colored and assigned consensus residue types by MVeiw (1). Sequences obtained from either Uniprot or Genbank. Uniprot accession numbers: NiV-F: Q9IH63, HeV-F: O89342, hPIV3-F: P06828, PIV5-F: P04849, MeV-F (ICB Strain): Q786F3, MojV-F: W8SKT3, CedV-F: J7GX38, hPIV1-F: P12605, NDV-F (Texas Strain): P26628, SeV-F (Z Strain): P04855. Genbank accession numbers: LayV-F: UUV47205.1, GakV-F: QYO90524.1, DarV-F: QYO90531.1.

References

1. Brown NP, Leroy C, Sander C. 1998. MView: a web-compatible database search or multiple alignment viewer. Bioinformatics 14:380-1.
2. Xu K, Chan Y-P, Bradel-Tretheway B, Akyol-Ataman Z, Zhu Y, Dutta S, Yan L, Feng Y, Wang L-F, Skiniotis G, Lee B, Zhou ZH, Broder CC, Aguilar HC, Nikolov DB. 2015. Crystal Structure of the Pre-fusion Nipah Virus Fusion Glycoprotein Reveals a Novel Hexamer-of-Trimers Assembly. PLOS Pathogens 11:e1005322.
3. Wong JJW, Paterson RG, Lamb RA, Jardetzky TS. 2016. Structure and stabilization of the Hendra virus F glycoprotein in its prefusion form. Proceedings of the National Academy of Sciences 113:1056-1061.
4. Stewart-Jones GBE, Chuang G-Y, Xu K, Zhou T, Acharya P, Tsybovsky Y, Ou L, Zhang B, Fernandez-Rodriguez B, Gilardi V, Silacci-Fregni C, Beltramello M, Baxa U, Druz A, Kong W-P, Thomas PV, Yang Y, Foulds KE, Todd J-P, Wei H, Salazar AM, Scorpio DG, Carragher B, Potter CS, Corti D, Mascola JR, Lanzavecchia A, Kwong PD. 2018. Structure-based design of a quadrivalent fusion glycoprotein vaccine for human parainfluenza virus types 1–4. Proceedings of the National Academy of Sciences 115:12265-12270.
5. Avanzato VA, Oguntuyo KY, Escalera-Zamudio M, Gutierrez B, Golden M, Kosakovsky Pond SL, Pryce R, Walter TS, Seow J, Doores KJ, Pybus OG, Munster VJ, Lee B, Bowden TA. 2019. A structural basis for antibody-mediated neutralization of Nipah virus reveals a site of vulnerability at the fusion glycoprotein apex. Proceedings of the National Academy of Sciences 116:25057-25067.
6. Dang HV, Cross RW, Borisevich V, Bornholdt ZA, West BR, Chan Y-P, Mire CE, Da Silva SC, Dimitrov AS, Yan L, Amaya M, Navaratnarajah CK, Zeitlin L, Geisbert TW, Broder CC, Veesler D. 2021. Broadly neutralizing antibody cocktails targeting Nipah virus and Hendra virus fusion glycoproteins. Nature Structural & Molecular Biology 28:426-434.
7. Pei J, Grishin NV. 2001. AL2CO: calculation of positional conservation in a protein sequence alignment. Bioinformatics 17:700-12.
8. Welch BD, Liu Y, Kors CA, Leser GP, Jardetzky TS, Lamb RA. 2012. Structure of the cleavage-activated prefusion form of the parainfluenza virus 5 fusion protein. Proceedings of the National Academy of Sciences 109:16672-16677.
9. Liu Q, Stone JA, Bradel-Tretheway B, Dabundo J, Benavides Montano JA, Santos-Montanez J, Biering SB, Nicola AV, Iorio RM, Lu X, Aguilar HC. 2013. Unraveling a Three-Step Spatiotemporal Mechanism of Triggering of Receptor-Induced Nipah Virus Fusion and Cell Entry. PLoS Pathogens 9:e1003770.
10. Loomis RJ, Stewart-Jones GBE, Tsybovsky Y, Caringal RT, Morabito KM, McLellan JS, Chamberlain AL, Nugent ST, Hutchinson GB, Kueltzo LA, Mascola JR, Graham BS. 2020. Structure-Based Design of Nipah Virus Vaccines: A Generalizable Approach to Paramyxovirus Immunogen Development. Frontiers in Immunology 11.
11. Dang HV, Chan Y-P, Park Y-J, Snijder J, Da Silva SC, Vu B, Yan L, Feng Y-R, Rockx B, Geisbert TW, Mire CE, Broder CC, Veesler D. 2019. An antibody against the F glycoprotein inhibits Nipah and Hendra virus infections. Nature Structural & Molecular Biology 26:980-987.
12. Punjani A, Rubinstein JL, Fleet DJ, Brubaker MA. 2017. cryoSPARC: algorithms for rapid unsupervised cryo-EM structure determination. Nature Methods 14:290-296.

13. Punjani A, Zhang H, Fleet DJ. 2020. Non-uniform refinement: adaptive regularization improves single-particle cryo-EM reconstruction. Nature Methods 17:1214-1221.
14. Lee JE, Fusco ML, Hessell AJ, Oswald WB, Burton DR, Saphire EO. 2008. Structure of the Ebola virus glycoprotein bound to an antibody from a human survivor. Nature 454:177-182.
15. Cai Y, Zhang J, Xiao T, Peng H, Sterling SM, Walsh RM, Rawson S, Rits-Volloch S, Chen B. 2020. Distinct conformational states of SARS-CoV-2 spike protein. Science 369:1586-1592.
16. Benton DJ, Nans A, Calder LJ, Turner J, Neu U, Lin YP, Ketelaars E, Kallewaard NL, Corti D, Lanzavecchia A, Gamblin SJ, Rosenthal PB, Skehel JJ. 2018. Influenza hemagglutinin membrane anchor. Proceedings of the National Academy of Sciences 115:10112-10117.
17. Ozorowski G, Pallesen J, de Val N, Lyumkis D, Cottrell CA, Torres JL, Copps J, Stanfield RL, Cupo A, Pugach P, Moore JP, Wilson IA, Ward AB. 2017. Open and closed structures reveal allostery and pliability in the HIV-1 envelope spike. Nature 547:360-363.
18. Kong R, Xu K, Zhou T, Acharya P, Lemmin T, Liu K, Ozorowski G, Soto C, Taft JD, Bailer RT, Cale EM, Chen L, Choi CW, Chuang G-Y, Doria-Rose NA, Druz A, Georgiev IS, Gorman J, Huang J, Joyce MG, Louder MK, Ma X, McKee K, O'Dell S, Pancera M, Yang Y, Blanchard SC, Mothes W, Burton DR, Koff WC, Connors M, Ward AB, Kwong PD, Mascola JR. 2016. Fusion peptide of HIV-1 as a site of vulnerability to neutralizing antibody. Science 352:828-833.
19. Pancera M, Zhou T, Druz A, Georgiev IS, Soto C, Gorman J, Huang J, Acharya P, Chuang G-Y, Ofek G, Stewart-Jones GBE, Stuckey J, Bailer RT, Joyce MG, Louder MK, Tumba N, Yang Y, Zhang B, Cohen MS, Haynes BF, Mascola JR, Morris L, Munro JB, Blanchard SC, Mothes W, Connors M, Kwong PD. 2014. Structure and immune recognition of trimeric pre-fusion HIV-1 Env. Nature 514:455-461.
20. Shi W, Cai Y, Zhu H, Peng H, Voyer J, Rits-Volloch S, Cao H, Mayer ML, Song K, Xu C, Lu J, Zhang J, Chen B. 2022. Cryo-EM structure of SARS-CoV-2 postfusion spike in membrane. bioRxiv doi:10.1101/2022.12.05.519151:2022.12.05.519151.
21. Zhang X-A, Li H, Jiang F-C, Zhu F, Zhang Y-F, Chen J-J, Tan C-W, Anderson DE, Fan H, Dong L-Y, Li C, Zhang P-H, Li Y, Ding H, Fang L-Q, Wang L-F, Liu W. 2022. A Zoonotic Henipavirus in Febrile Patients in China. New England Journal of Medicine 387:470-472.
22. Wu Z, Yang L, Yang F, Ren X, Jiang J, Dong J, Sun L, Zhu Y, Zhou H, Jin Q. 2014. Novel Henipa-like virus, Mojiang Paramyxovirus, in rats, China, 2012. Emerg Infect Dis 20:1064-6.
23. Lee S-H, Kim K, Kim J, No JS, Park K, Budhathoki S, Lee SH, Lee J, Cho SH, Cho S, Lee G-Y, Hwang J, Kim H-C, Klein TA, Uhm C-S, Kim W-K, Song J-W. 2021. Discovery and Genetic Characterization of Novel Paramyxoviruses Related to the Genus Henipavirus in Crocidura Species in the Republic of Korea. Viruses 13:2020.
24. Field H, Young P, Yob JM, Mills J, Hall L, Mackenzie J. 2001. The natural history of Hendra and Nipah viruses. Microbes Infect 3:307-14.
25. Rima B, Balkema-Buschmann A, Dundon WG, Duprex P, Easton A, Fouchier R, Kurath G, Lamb R, Lee B, Rota P, Wang L, Ictv Report C. 2019. ICTV Virus Taxonomy Profile: Paramyxoviridae. J Gen Virol 100:1593-1594.

26. Anonymous. Prioritizing diseases for research and development in emergency contexts, *on* WHO. https://www.who.int/activities/prioritizing-diseases-for-research-and-development-in-emergency-contexts. Accessed 2/28/23.
27. Aguilar HC, Iorio RM. 2012. Henipavirus Membrane Fusion and Viral Entry, p 79-94. *In* Lee B, Rota PA (ed), Henipavirus: Ecology, Molecular Virology, and Pathogenesis doi:10.1007/82_2012_200. Springer Berlin Heidelberg, Berlin, Heidelberg.
28. Negrete OA, Levroney EL, Aguilar HC, Bertolotti-Ciarlet A, Nazarian R, Tajyar S, Lee B. 2005. EphrinB2 is the entry receptor for Nipah virus, an emergent deadly paramyxovirus. Nature 436:401-5.
29. Xu K, Rajashankar KR, Chan Y-P, Himanen JP, Broder CC, Nikolov DB. 2008. Host cell recognition by the henipaviruses: Crystal structures of the Nipah G attachment glycoprotein and its complex with ephrin-B3. Proceedings of the National Academy of Sciences 105:9953-9958.
30. White JM, Delos SE, Brecher M, Schornberg K. 2008. Structures and mechanisms of viral membrane fusion proteins: multiple variations on a common theme. Crit Rev Biochem Mol Biol 43:189-219.
31. Lamb RA, Jardetzky TS. 2007. Structural basis of viral invasion: lessons from paramyxovirus F. Current Opinion in Structural Biology 17:427-436.
32. Pager CT, Dutch RE. 2005. Cathepsin L is involved in proteolytic processing of the Hendra virus fusion protein. J Virol 79:12714-20.
33. Bose S, Jardetzky TS, Lamb RA. 2015. Timing is everything: Fine-tuned molecular machines orchestrate paramyxovirus entry. Virology 479-480:518-31.
34. Iorio RM, Melanson VR, Mahon PJ. 2009. Glycoprotein interactions in paramyxovirus fusion. Future Virol 4:335-351.
35. Hsieh C-L, Goldsmith JA, Schaub JM, DiVenere AM, Kuo H-C, Javanmardi K, Le KC, Wrapp D, Lee AG, Liu Y, Chou C-W, Byrne PO, Hjorth CK, Johnson NV, Ludes-Meyers J, Nguyen AW, Park J, Wang N, Amengor D, Lavinder JJ, Ippolito GC, Maynard JA, Finkelstein IJ, McLellan JS. 2020. Structure-based design of prefusion-stabilized SARS-CoV-2 spikes. Science 369:1501-1505.
36. Wrapp D, Wang N, Corbett KS, Goldsmith JA, Hsieh C-L, Abiona O, Graham BS, McLellan JS. 2020. Cryo-EM structure of the 2019-nCoV spike in the prefusion conformation. Science 367:1260-1263.
37. Do Kwon Y, Pancera M, Acharya P, Georgiev IS, Crooks ET, Gorman J, Joyce MG, Guttman M, Ma X, Narpala S, Soto C, Terry DS, Yang Y, Zhou T, Ahlsen G, Bailer RT, Chambers M, Chuang G-Y, Doria-Rose NA, Druz A, Hallen MA, Harned A, Kirys T, Louder MK, O'Dell S, Ofek G, Osawa K, Prabhakaran M, Sastry M, Stewart-Jones GBE, Stuckey J, Thomas PV, Tittley T, Williams C, Zhang B, Zhao H, Zhou Z, Donald BR, Lee LK, Zolla-Pazner S, Baxa U, Schön A, Freire E, Shapiro L, Lee KK, Arthos J, Munro JB, Blanchard SC, Mothes W, Binley JM, et al. 2015. Crystal structure, conformational fixation and entry-related interactions of mature ligand-free HIV-1 Env. Nature Structural & Molecular Biology 22:522-531.
38. Rawi R, Rutten L, Lai Y-T, Olia AS, Blokland S, Juraszek J, Shen C-H, Tsybovsky Y, Verardi R, Yang Y, Zhang B, Zhou T, Chuang G-Y, Kwong PD, Langedijk JPM. 2020. Automated Design by Structure-Based Stabilization and Consensus Repair to Achieve Prefusion-Closed Envelope Trimers in a Wide Variety of HIV Strains. Cell Reports 33:108432.

39. Tan YZ, Baldwin PR, Davis JH, Williamson JR, Potter CS, Carragher B, Lyumkis D. 2017. Addressing preferred specimen orientation in single-particle cryo-EM through tilting. Nature Methods 14:793-796.
40. Hashiguchi T, Fukuda Y, Matsuoka R, Kuroda D, Kubota M, Shirogane Y, Watanabe S, Tsumoto K, Kohda D, Plemper RK, Yanagi Y. 2018. Structures of the prefusion form of measles virus fusion protein in complex with inhibitors. Proceedings of the National Academy of Sciences 115:2496-2501.
41. Yin HS, Wen X, Paterson RG, Lamb RA, Jardetzky TS. 2006. Structure of the parainfluenza virus 5 F protein in its metastable, prefusion conformation. Nature 439:38-44.
42. Murray K, Selleck P, Hooper P, Hyatt A, Gould A, Gleeson L, Westbury H, Hiley L, Selvey L, Rodwell B, Ketterer P. 1995. A Morbillivirus that Caused Fatal Fisease in Horses and Humans. Science 268:94-97.
43. Madera S, Kistler A, Ranaivoson HC, Ahyong V, Andrianiaina A, Andry S, Raharinosy V, Randriambolamanantsoa TH, Ravelomanantsoa NAF, Tato CM, DeRisi JL, Aguilar HC, Lacoste V, Dussart P, Heraud J-M, Brook CE. 2022. Discovery and Genomic Characterization of a Novel Henipavirus, Angavokely Virus, from Fruit Bats in Madagascar. Journal of Virology 96:e00921-22.
44. Hernández LHA, da Paz TYB, Silva SPd, Silva FSd, Barros BCVd, Nunes BTD, Casseb LMN, Medeiros DBA, Vasconcelos PFdC, Cruz ACR. 2022. First Genomic Evidence of a Henipa-like Virus in Brazil. Viruses 14:2167.
45. Aguilar HC, Matreyek KA, Filone CM, Hashimi ST, Levroney EL, Negrete OA, Bertolotti-Ciarlet A, Choi DY, McHardy I, Fulcher JA, Su SV, Wolf MC, Kohatsu L, Baum LG, Lee B. 2006. N-glycans on Nipah virus fusion protein protect against neutralization but reduce membrane fusion and viral entry. J Virol 80:4878-89.
46. Carter JR, Pager CT, Fowler SD, Dutch RE. 2005. Role of N-linked glycosylation of the Hendra virus fusion protein. J Virol 79:7922-5.
47. Yin H-S, Paterson RG, Wen X, Lamb RA, Jardetzky TS. 2005. Structure of the uncleaved ectodomain of the paramyxovirus (hPIV3) fusion protein. Proceedings of the National Academy of Sciences 102:9288-9293.
48. Yeo YY, Buchholz DW, Gamble A, Jager M, Aguilar HC. 2021. Headless Henipaviral Receptor Binding Glycoproteins Reveal Fusion Modulation by the Head/Stalk Interface and Post-receptor Binding Contributions of the Head Domain. Journal of Virology 95:e00666-21.
49. Bose S, Heath CM, Shah PA, Alayyoubi M, Jardetzky TS, Lamb RA. 2013. Mutations in the parainfluenza virus 5 fusion protein reveal domains important for fusion triggering and metastability. J Virol 87:13520-31.
50. Poor TA, Jones LM, Sood A, Leser GP, Plasencia MD, Rempel DL, Jardetzky TS, Woods RJ, Gross ML, Lamb RA. 2014. Probing the paramyxovirus fusion (F) protein-refolding event from pre- to postfusion by oxidative footprinting. Proceedings of the National Academy of Sciences 111:E2596-E2605.
51. Wilman HR, Shi J, Deane CM. 2014. Helix kinks are equally prevalent in soluble and membrane proteins. Proteins 82:1960-70.
52. McCarthy KR, Lee J, Watanabe A, Kuraoka M, Robinson-McCarthy LR, Georgiou G, Kelsoe G, Harrison SC. 2021. A Prevalent Focused Human Antibody Response to the Influenza Virus Hemagglutinin Head Interface. mBio 12:e01144-21.

53. Grant T, Grigorieff N. 2015. Measuring the optimal exposure for single particle cryo-EM using a 2.6 Å reconstruction of rotavirus VP6. Elife 4:e06980.
54. Liebschner D, Afonine PV, Baker ML, Bunkoczi G, Chen VB, Croll TI, Hintze B, Hung L-W, Jain S, McCoy AJ, Moriarty NW, Oeffner RD, Poon BK, Prisant MG, Read RJ, Richardson JS, Richardson DC, Sammito MD, Sobolev OV, Stockwell DH, Terwilliger TC, Urzhumtsev AG, Videau LL, Williams CJ, Adams PD. 2019. Macromolecular structure determination using X-rays, neutrons and electrons: recent developments in Phenix. Acta Crystallographica Section D 75:861-877.
55. Anonymous. The PyMOL Molecular Graphics System, v2.0. Schrödinger, LLC,
56. Pettersen EF, Goddard TD, Huang CC, Meng EC, Couch GS, Croll TI, Morris JH, Ferrin TE. 2021. UCSF ChimeraX: Structure visualization for researchers, educators, and developers. Protein Sci 30:70-82.
57. Croll T. 2018. ISOLDE: a physically realistic environment for model building into low-resolution electron-density maps. Acta Crystallographica Section D 74:519-530.
58. Madeira F, Pearce M, Tivey ARN, Basutkar P, Lee J, Edbali O, Madhusoodanan N, Kolesnikov A, Lopez R. 2022. Search and sequence analysis tools services from EMBL-EBI in 2022. Nucleic acids research doi:10.1093/nar/gkac240:gkac240.

Acknowledgments

Cryo-EM data were collected at the Duke Krios at the Duke University Shared Materials Instrumentation Facility (SMIF), a member of the North Carolina Research Triangle Nanotechnology Network (RTNN), which is supported by the National Science Foundation (award number ECCS-2025064) as part of the National Nanotechnology Coordinated Infrastructure (NNCI). This study utilized the computational resources offered by Duke Research Computing (http://rc.duke.edu; NIH 1S10OD018164-01) at Duke University. This work was supported by funding from the Translating Duke Health Initiative. The comparative analysis of diverse Class I fusion peptides was supported in part by funding from NIAID grant R01 AI145687, R01 AI165947 and U54 AI170752. Figure 5 was made using BioRender.

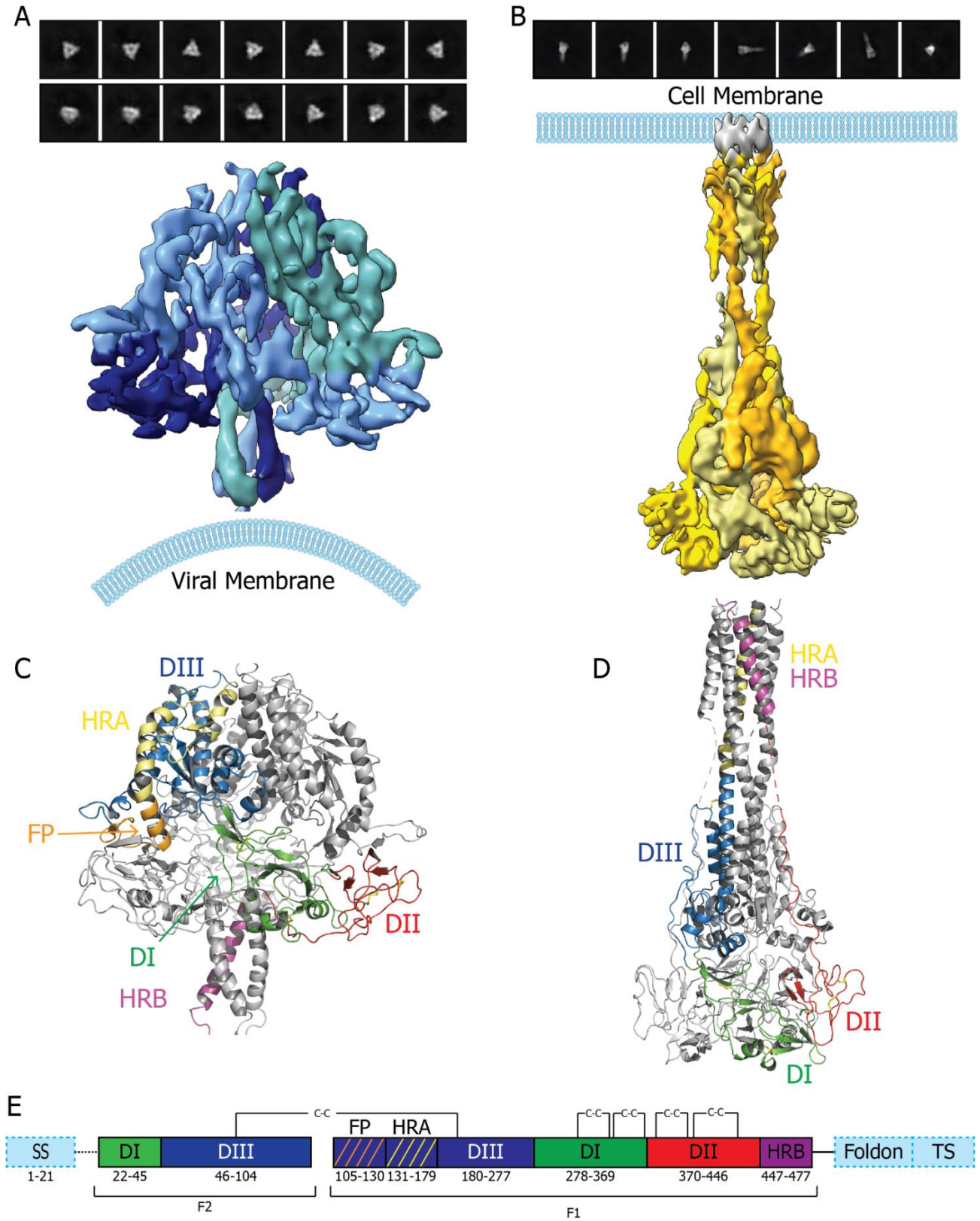

Figure 1: Structures of LayV-F in pre- and post-fusion conformation:

A-B. Cryo-EM reconstructions of LayV-F in **A.** pre- and **B.** post-fusion conformation, colored by protomer. Map regions colored in different shades of blue (pre-fusion) and yellow (post-fusion) for each protomer. Representative reference-free 2D classes used for the reconstruction are displayed above each map. **C-D.** Cartoon representation of atomic models of LayV-F in **C.** pre-fusion and **D.** post-fusion conformation that were built into the maps shown in **A-B**. In each, one protomer is colored by domain, based on the color scheme in panel **E**, and the other two protomers colored gray. **E.** Sequence domain key for LayV-F. SS: Secretion signal, cleaved prior to purification. DI, DII, DIII: Domains I, II, and III. FP: Fusion Peptide. HRA, HRB: Heptad repeats A and B. Foldon: Trimerization domain. TS: Twin-Strep tag, used for purification with modified streptavidin resin.

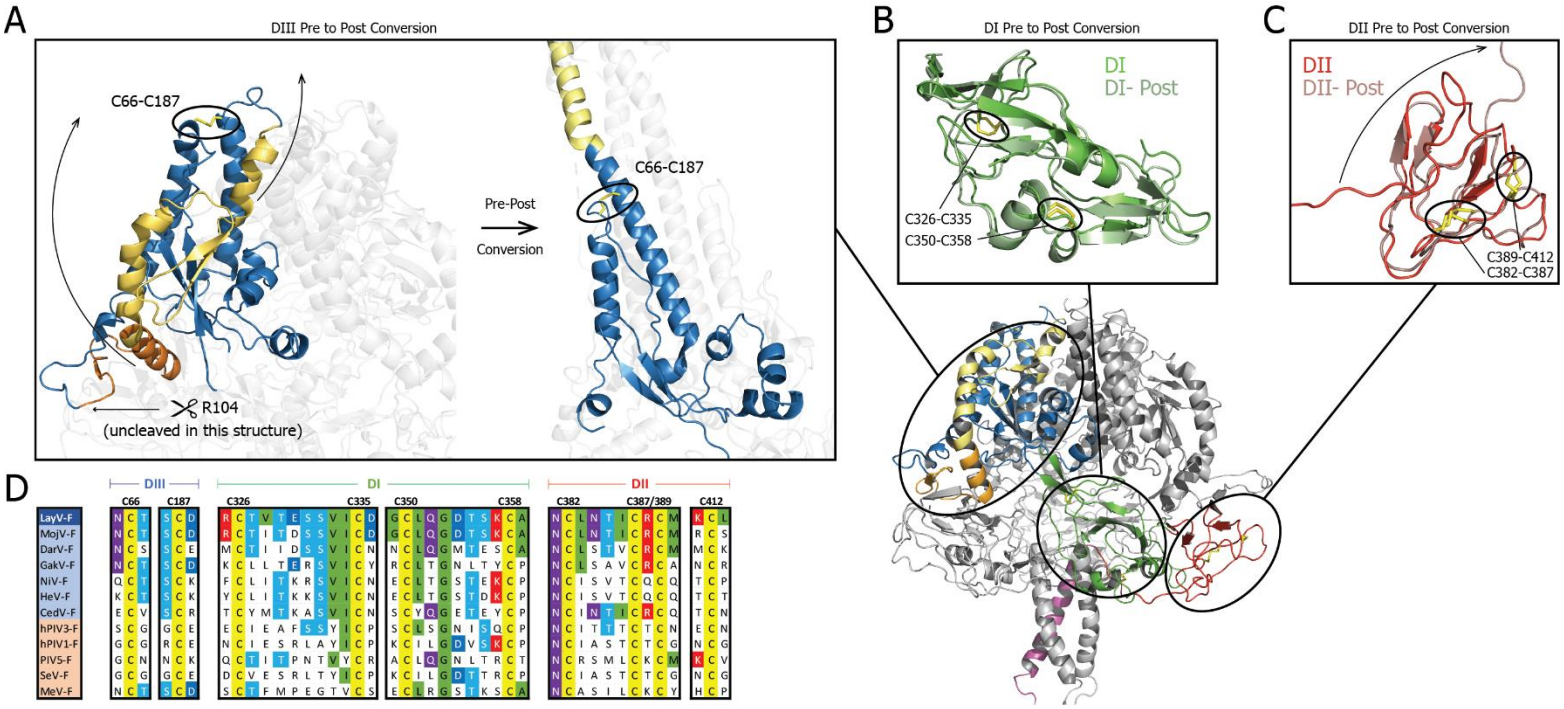

Figure 2: Role of conserved cysteines during conformational conversion.

A. Zoomed-in view of the DIII domain, including the fusion peptide (orange) and HRA (yellow), shown for the (left) pre- and (right) post-fusion structures. Color scheme continued from Figure 1E. The cleavage site at R104 is identified, as well as the disulfide bond formed by C66 and C187 (yellow sticks). This disulfide bond is a hinge point around which the HRA straightens into the central coiled-coil in the post-fusion F structure. **B-C.** Superimposition of pre- and post-fusion conformation domains DI (**B**) and DII (**C**). Color scheme continued from figure 1E, with the post-fusion conformation colored in a lighter shade. Disulfide bonds are shown as yellow sticks and labelled. For DII, the movement of the HRB linker region is indicated by an arrow. **D.** Sequence alignment of paramyxovirus fusion proteins in the regions surrounding conserved cysteines, with cysteine residue number and domain labelled. Viruses colored blue are from the *Henipavirus* genus and colored tan for other paramyxoviruses. Residues are colored by type, per MView standard (1). Blue: Alcohol, Green: Hydrophobic, Dark Blue: Negative charge, Red: Positive charge, Purple: Polar, Yellow: Cysteine.

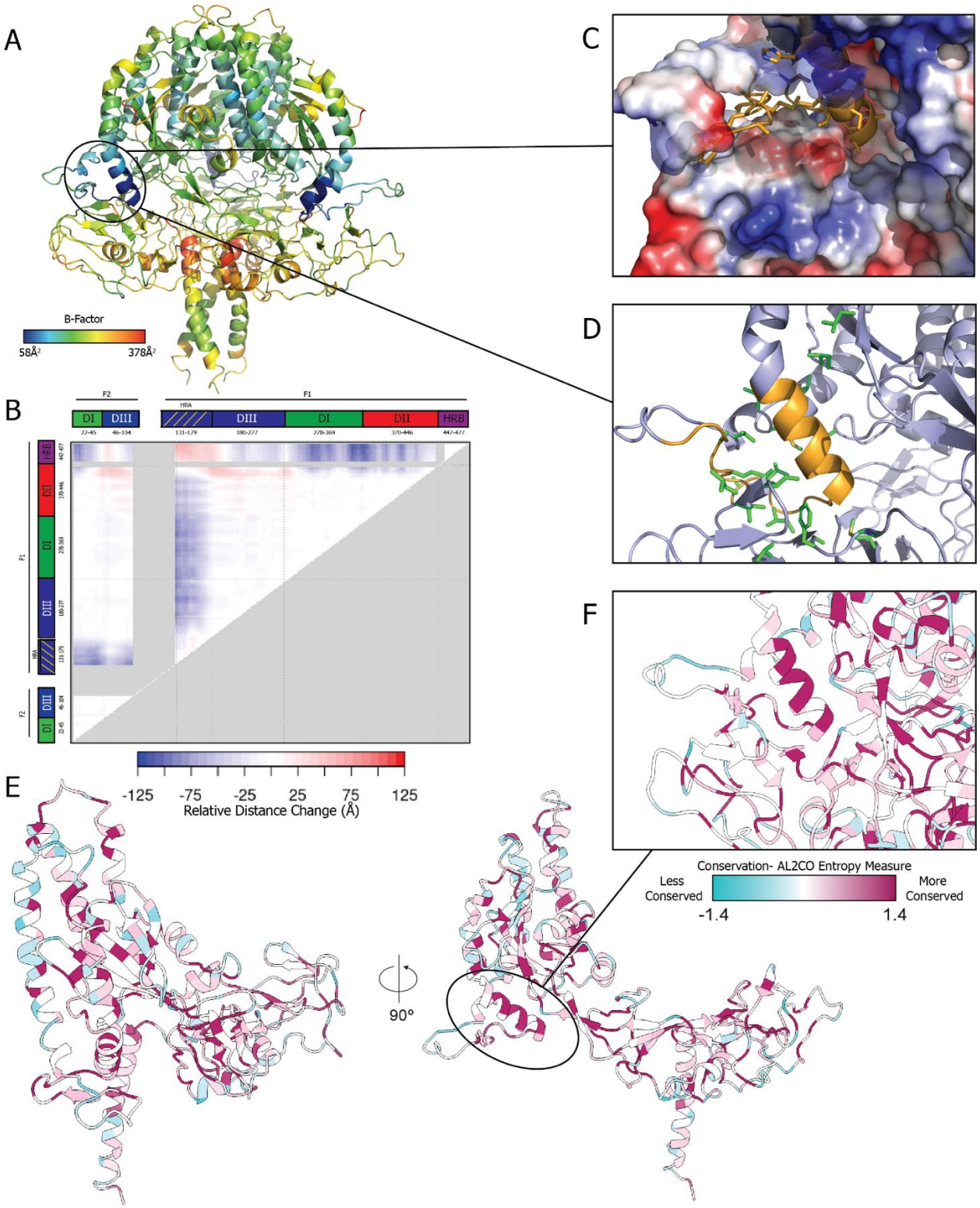

Figure 3: Fusion peptide burial and conservation.

A. Structure of the pre-fusion LayV-F protein shown in cartoon representation and colored by B-factors. **B.** Difference Distance Matrix plot comparing relative residue positions between pre-fusion and post-fusion conformation. Sequence key from figure 1E included along each axis. Gray areas in the bottom right half of the plot are the result of sequences not present in the post-fusion model. **C.** Hydrophobic fusion peptide pocket in pre-fusion state, with fusion peptide depicted as orange cartoon, and surface electrostatics view of the pocket. **D.** Side-chain stick view of the fusion peptide pocket, with hydrophobic residues involved shown with side chains as green sticks. An enlarged view of this panel with residues labeled is seen in supplemental figure S5. **E.** Cartoon representations of a single pre-fusion state protomer, colored by sequence conservation across *Henipavirus* fusion proteins. Color scale generated by ChimeraX default AL2CO entropy measure. **F.** Zoom in of the fusion peptide pocket, colored by sequence conservation as in H. The fusion peptide pocket is among the most strongly conserved region of the protein.

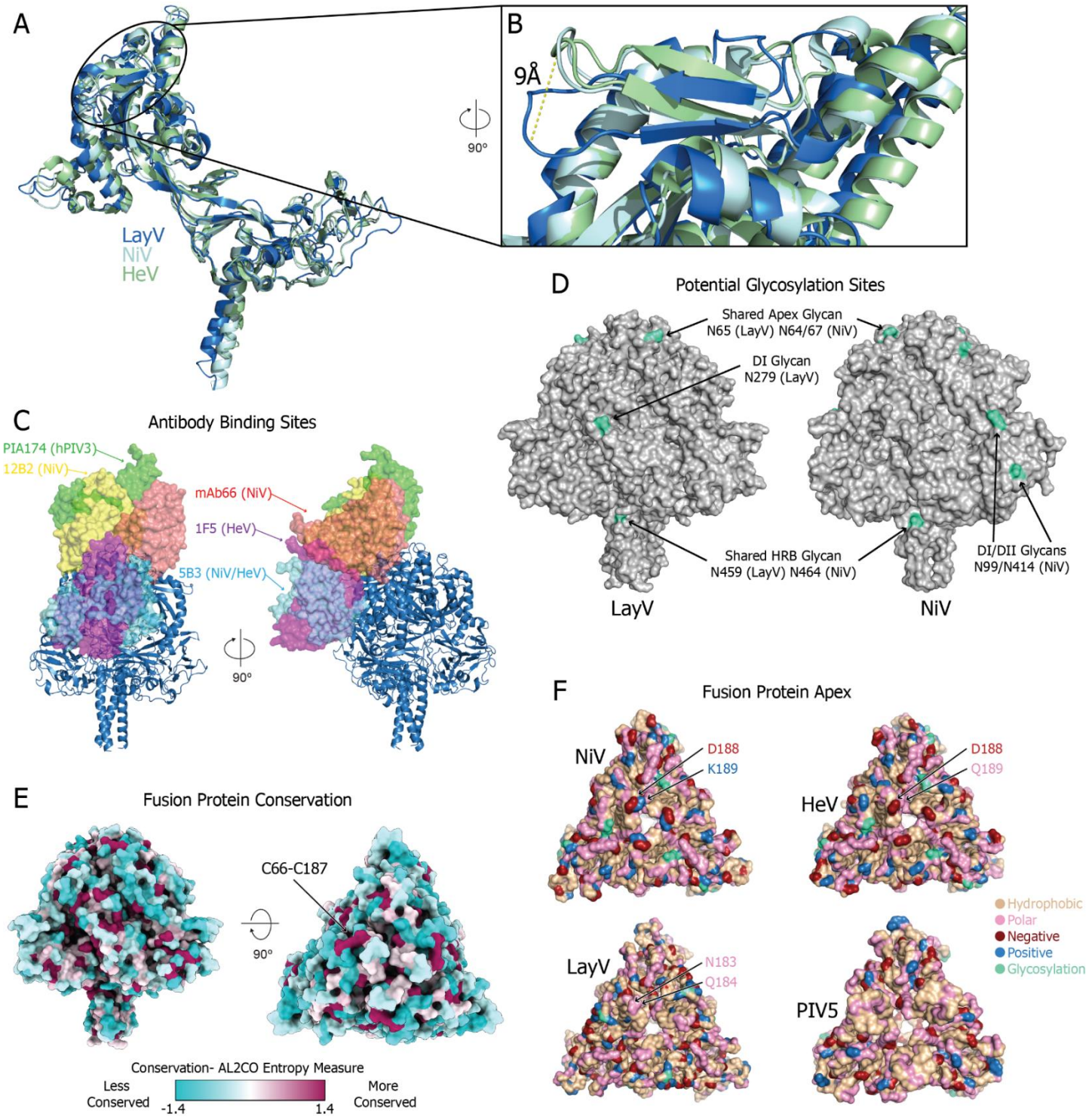

Figure 4: Structure and antigenicity comparison of Henipavirus fusion proteins.

A. Superimposition of a single pre-fusion protomer of LayV-F (blue) NiV-F (cyan) and HeV-F (green), in cartoon representation. PDBs: LayV-F: 8FEJ, NiV-F: 5EVM, HeV-F: 5EJB (2, 3). **B.** Zoomed in view of a loop within the folded HRA, one of the few areas of significant structural difference between LayV-F and NiV/HeV-F. **C.** Binding site of known paramyxovirus F protein-neutralizing antibodies, labeled by the species targeted. NiV-F trimer from 12B2-bound structure shown as cartoon and antibody Fabs shown in surface view. Only one Fab per type shown, all expect PIA174 bind with 3:1 stoichiometry. PDBs: PIA174: 6MJZ, 12B2: 7KI4, mAb66: 6T3F, 1F5: 7KI6, 5B3: 6TYS (4-6). **D.** Surface view of LayV-F and NiV-F with glycosylation sites (residues meeting the N-X-S/T glycosylation sequence) colored teal. **E.** Surface representation of LayV-F colored by sequence conservation across *Henipavirus* fusion proteins. Color scale generated by ChimeraX default AL2CO entropy measure; magenta indicates high conservation and teal indicates high variability (7). **F.** Surface representation of paramyxovirus fusion proteins, showing only main chain atoms, colored by residue type and shown from top-down view. Tan: hydrophobic, Pink: polar, Red: negative, Blue: positive, teal: Potential glycosylation. PIV5 PBD: 4GIP (8).

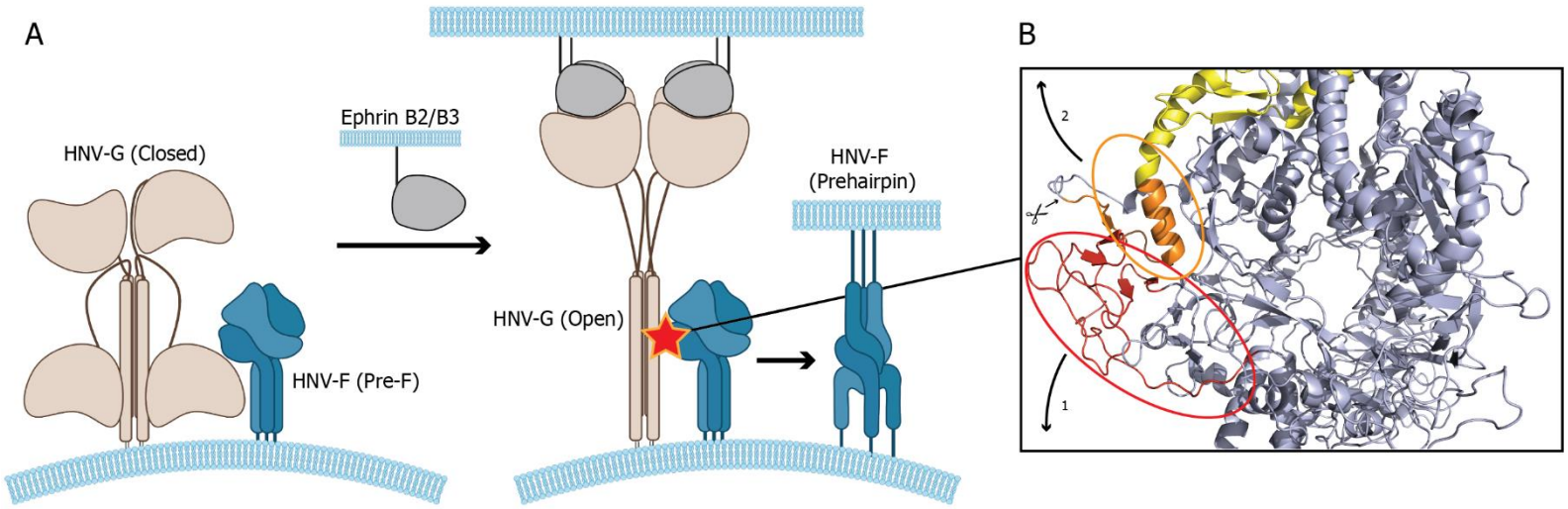

Figure 5: Fusion triggering hypothesis for paramyxoviruses.

A. Existing model of *Henipavirus* (HNV) fusion protein triggering based on Liu *et al.* (2013) (9). HNV-G, brown, shown in a two-receptor binding domain down "closed" state, bound to HNV-F in pre-fusion conformation. Exposure to Ephrin B2/B3 receptor induces opening of HNV-G, triggering conversion of HNV-F from pre-fusion to the pre-hairpin state. The triggering interaction is labeled with a star. **B.** Hypothesized structural basis for the G-F interaction shown in **A**, wherein a two-step mechanism involving disruption of the fusion peptide burial pocket through action of the HNV-G stalk on DII frees the fusion peptide, allowing conformational conversion.